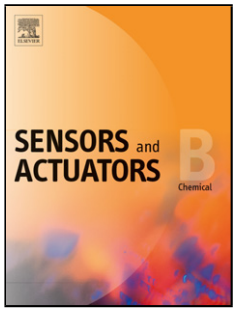

Title: Versatile digital polymerase chain reaction chip design, fabrication, and image processing

Authors: Huanan Li, Haoqing Zhang, Ying Xu, Alzbeta Tureckova, Pavel Zahradník, Honglong Chang, Pavel Neuzil

PII: S0925-4005(18)32191-9
DOI: https://doi.org/10.1016/j.snb.2018.12.072
Reference: SNB 25833

To appear in: *Sensors and Actuators B*

Received date: 13 August 2018
Revised date: 24 November 2018
Accepted date: 13 December 2018

Please cite this article as: Li H, Zhang H, Xu Y, Tureckova A, Zahradník P, Chang H, Neuzil P, Versatile digital polymerase chain reaction chip design, fabrication, and image processing, *Sensors and amp; Actuators: B. Chemical* (2018), https://doi.org/10.1016/j.snb.2018.12.072

Versatile digital polymerase chain reaction chip design, fabrication, and image processing

Huanan Li[1], Haoqing Zhang[1], Ying Xu[1], Alzbeta Tureckova[1,2], Pavel Zahradník[1,3], Honglong Chang[1*], and Pavel Neuzil[1*]

[1]Northwestern Polytechnical University, Department of Microsystems, Faculty of Mechanical Engineering, 127 West Youyi Road, Xi'an, 710072 Shaanxi, P.R. China
[2]Tomas Bata University in Zlin, Faculty of Applied Informatics, Nam T.G. Masaryka 5555, 760 01 Zlin, Czech Republic
[3]Czech Technical University in Prague, Faculty of Electrical Engineering, Department of Telecommunications Engineering, Technicka 1902/2, 166 27 Czech Republic
[4]Brno University of Technology, Faculty of Electrical Engineering and Communication, SIX Centre, Department of Microelectronics, Technická 3058/10, 61600 Brno, Czech Republic
[*]corresponding authors

Highlights

- A family of 4 digital PCR chips with wells numbers from 26 448 to 1 656 000
- All layouts have the same layout philosophy.
- The layout is split into 6 fields each captured by a single shoot
- Image processing swift and convenient with a user friendly interface.
- The dPCR can detect circulating tumor DNA molecules.
- Fluorescence image processing applicable for array-based microfluidics

Abstract

We present a family of digital polymerase chain reaction (dPCR) chips made of silicon that that are (9 × 9) mm^2 in size, have a unique layout design, and have between 26,448 and 1,656,000 reaction wells. The chip layout was split into six fields sized 4200 × 2785 μm^2 that contain reaction wells with a gap of a few µm separating the fields from each other. We also developed a universal fluorescence imaging method capable of processing images from those chips. It comprised automatic image acquisition, image stitching, alignment mark registration, rotation correction, determination of reaction wells' positions, and result processing. The chip design, with fully automated image processing, provided a fast and reliable system for the absolute quantitative analysis of dPCR. Combined with ease-of-use, this family of dPCR chip offers a pathway to enable fast and affordable digital microfluidic diagnostic applications.

Keywords: digital PCR, silicon chip, fluorescence image analysis, DNA counting, microfluidic chip array

1. Introduction

The polymerase chain reaction (PCR) method [1] is an effective technique for multiplying an amplicon of deoxyribonucleic acid (DNA) with a specific sequence via thermal cycling in a "PCR master mix" solution. It contains the target DNA template; polymerase; deoxyribonucleoside triphosphate (dNTP); forward and reverse primers specific to the target DNA; a bivalent salt, such as $MgCl_2$; and a buffer to adjust the solution's pH. The PCR results are detected either in real time [2, 3] using intercalating dyes, probes, or other fluorescence methods, or as an endpoint detection using ethidium bromide combined with electrophoresis. There are many PCR techniques, including one called "digital PCR" (dPCR) [4].

In recent years, dPCR has attracted significant attention due to its ability to achieve an absolute quantification of target DNA molecules. More importantly, dPCR can also detect rare DNA, even if there is also an abundance of non-target DNA [5-11]. This is not possible when using a conventional PCR technique. In dPCR, the original sample is split into thousands of partitions, each containing either one or none of the target DNA molecules. Once the thermal cycling is complete, the partitions containing the target DNA molecules are counted based on their fluorescence amplitude, thus providing an absolute quantification of the original sample. In recent years, dPCR technology has become a powerful tool [12] for prenatal diagnosis [13], the detection of gene mutations [14], and early cancer detection [15-18]. There are two basic systems for performing dPCR: droplet (ddPCR) and chip-based (cdPCR).

Sample processing in the ddPCR system starts with the formation of an emulsion of droplets containing the PCR master mix and one (or no) target DNA molecules in each droplet. Thermal cycling is then performed (PCR) and the number of droplets containing the target DNA molecules is then counted using flow cytometry.

In contrast, the sample in the cdPCR system is loaded directly into the reaction wells within the chip prior to thermal cycling and final processing by fluorescence imaging. The methods of cdPCR image processing are typically derived from existing fluorescence imaging techniques used primarily for microarrays consisting of reaction spots and their defined boundaries ("grids") where the amplitude of fluorescence from individual spots is typically represented as a level of gray [19-22]. The captured image must be split into segments, which makes the analysis simpler and the locating of the spots and their boundaries easier. There are numerous image segmentation algorithms and methods [23, 24]. These are typically based on defining a threshold, regions, and edges and involve morphological tools [25], clustering [26], adaptive procedures [27], K-mean clustering [28], statistical confidence intervals [29], convolutional neural networks [30], and deep learning [31].

Once the segmentation is complete, a method called "grid division" (lines) can effectively eliminate the mutual influence of adjacent points in the microarray image via noise suppression [32]. This method relies on regular gridding and segmentation [33] or an original genetic algorithm for grid pre-processing [34]. The results can be affected by a high amplitude of noise within the image, however, and these two methods also lack sufficient stability for the automatic image processing. The numerical image processing technique used to track interface spot movement in microarrays is called the "level set method" and is based on a combination of Chan–Vase approximation and the Mumford–Shan model [35]. This technique can process the image irrespective of the spot shape and noise intensity. Nevertheless, it is easy to miss a spot if its fluorescence amplitude level is close to the level of the background noise.

Determination of reaction spots' locations in the microarray is conducted using a grid division method. Its precision be affected by noise and other interference that causes redundancy or missing grid lines. Additionally, overlapping reaction spot regions in adjacent rows and columns can occur in arrays with high spot density. An automated method to calculate the fluorescence intensity in reaction wells was introduced [36] with a condition

that reaction wells found 15 or more pixels away from their expected location would not be included in the analysis.

Here, we show a family of cdPCR chips with a unique design where the areas with the reaction wells are split into six blocks and alignment marks to simplify further image processing. We also propose a method to seal individual wells from each other to suppress well-to-well cross-contamination. The proposed image processing method has the following advantages compared to the other cdPCR image analysis methods: (1) it is fast and fully automated; (2) it accurately determines the reaction wells' locations; (3) it performs fast fluorescence intensity analysis, resulting in high throughput; and (4) the method can be used to develop tools in the laboratory and for commercial instruments. The image processing starts with image acquisition followed by image stitching, alignment mark registration, rotation correction, reaction well positioning, and fluorescence intensity statistics and results in an accurate count of DNAs using a user-friendly interface. It is suitable for further system miniaturization for economical systems making dPCR technique affordable in a similar fashion as shown earlier for miniaturized lab-on-a-chip [37] and real-time PCR systems[38-40].

2. Materials and Methods

2.1. Chip design and fabrication

The dPCR chips were ≈ (9 × 9) mm^2 in size with reaction well diameters of 5 μm, 10 μm, 20 μm, and 50 μm and were designed using the script-based Nanolithography Toolbox [41] with the aim of having a unified system for further image processing. The area occupied by the reaction wells was split into six blocks ≈ (4.2 × 2.8) mm^2 in size and fit into the field of view of a fluorescence microscope equipped with a 2.5× lens and a complementary metal oxide semiconductor (CMOS) camera imager. The camera imager was ≈ (22.5 × 15.0) mm^2 in size with 5470 × 3648 pixels. This corresponded to ≈ 20.2 million pixels with a pixel pitch of 4.1 μm according to the manufacturer's datasheet. Each block was formed using hexagonal arrays and this was scripted using <hexHole> cell to create a block of wells with a parameter specific to the well diameter. An array with the size of 2 × 3 was placed into the layout with a stepping distance of 4205 μm × 2792 μm.

The design was also equipped with six alignment marks for further image processing. These marks were crosses <cross> placed symmetrically at the chip perimeter with set stepping distances of 8700 μm and 4350 μm in the X and Y directions, respectively. Finally, the chip included test structures scripted using <resoPatternRSA> and <resoPatternLSA> to verify the lithography performance, such as lines and corners with different widths. The script for the chip design with 50 μm wells is in supplementary section.

Chip fabrication was conducted using a silicon wafer with a diameter of ≈ 100 mm and crystallographic orientation of (100) using contact lithography. The wafer was first coated with a self-assembly monolayer of hexamethylene disilazane inside a vacuum chamber. Then, the wafer was spun with positive photoresist (PR) with a target thickness of 2.3 μm and pre-baked at a hotplate temperature of ≈ 80°C for ≈ 60 s. The wafer was exposed to ultraviolet radiation through a chrome mask, post-baked at ≈ 110°C for ≈ 180 s, and developed for ≈ 60 s in a tetramethylammonium hydroxide-based developer. The wafer was then washed with deionized (DI) water, dried by N_2, and etched using a deep reactive ion etching (Bosch) process [42] into target depths of 50, 20, 10, and 5 μm depending on the design. Then, the PR was removed and the wafer was partitioned into individual chips using a diamond-blade dicing saw. Finally, the chips were loaded with the PCR master mix sample and sealed using a glass lid covered with PDMS and parylene to suppress sample evaporation during the thermal cycling (Figure 1A).

2.2. dPCR chip surface treatment and sample loading

We cleaned and oxidized the silicon chip surface using oxygen plasma at a power of ≈ 90 W for ≈ 120 s to make the surface clean and hydrophilic to improve the PCR master mix loading efficiency. Then, we loaded the PCR master mix into the wells using a blade technique. We pipetted ≈ 3 µL of the PCR master mix onto the edge of the chip and used a plastic blade to evenly distribute the solution into the reaction wells. The chip was subsequently covered with a glass microscope cover slip $\approx (10 \times 10)\ \mathrm{mm}^2$ in size and coated with polydimethylsiloxane (PDMS) and parylene-C to suppress PCR master mix evaporation and to limit well-to-well cross-contamination during the thermal cycling. The hydrophobic and soft nature of the glass cover slip coated with parylene over the PDMS layer prevented the solution from one well contaminating the solution in the neighboring wells. We then placed the chip on the thermo-electric cooler (TEC) on the X–Y stage of a microscope with a temperature sensor mounted to the TEC surface (Figure 1D).

2.3. Fluorescence signal detection and analysis method

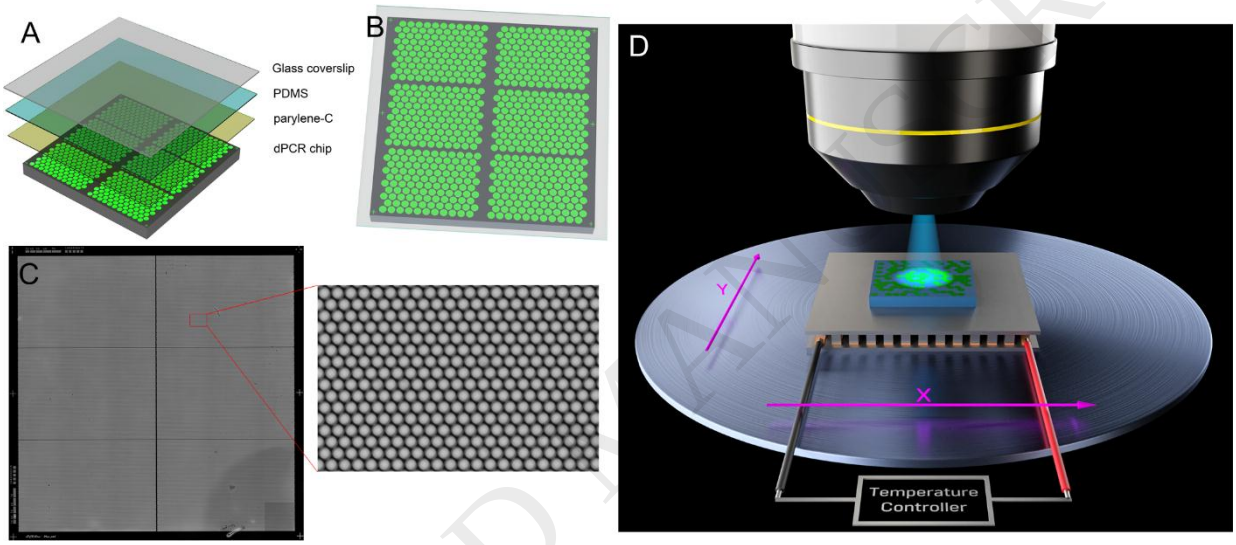

Figure 1 Schematic of the cdPCR system. (A) Schematic of the layered chip packaging structure. The non-volatile cover is formed by the bonding of the glass and the polydimethylsiloxane (PDMS) and then coated with a layer of parylene-C. (B) Schematic of the entire sealed microfluidic chip with alignment marks on the edge of the chip. (C) Fluorescent image of a dPCR chip with wells 20 µm in diameter filled with fluorescein captured by a camera attached to the c-mount port of an optical microscope. (D) Schematic representation of the cdPCR system setup showing the cdPCR chip placed on TEC on the X–Y microscope stage. The temperature of the top plate of the TEC was controlled using a closed feedback loop system based on the signal from a temperature sensor placed next to the dPCR chip. The proportional integrative derivative control method was performed using a custom-made script in a LabView environment. Once the temperature cycling was completed, we captured an image of the chip using an optical microscope in fluorescence mode.

All methods used for the digital image processing of the microscopic images were chosen primarily based on their real-time capability. We intentionally applied established robust and deterministic algorithms with the ability to parallel process on multi-core computing structures. Therefore, we avoided new but unproved or non-deterministic algorithms like deep learning, etc.

The algorithm for the dPCR chip fluorescence signal detection and analysis method started by capturing images of the dPCR chip. These were divided into blocks and imaged using a method determined by the number of reaction wells (described in Section 3.3.1). Then, we performed the image pre-processing using the algorithm,

including the six alignment marks' registration (identification) and localization using the Canny edge operator and Hough transform method, rotation correction based on the calculated angle of rotation from the registered alignment marks, and the resizing of the image into the designed size. Subsequently, the fluorescence signal of the corrected fluorescence image was extracted and analyzed by the creation of a label matrix, signal extraction, and data normalization (Figure 2).

2.4. Fluorescence image acquisition of the dPCR chip

The field of view of the microscope projected at the camera CMOS imager did not cover the entire dPCR chip area, therefore, we performed multiple acquisitions of the fluorescence images covering part of the chip (partial image) to obtain the image of the entire dPCR chip (complete image) using either a block or stitching method.

Method 1: Block

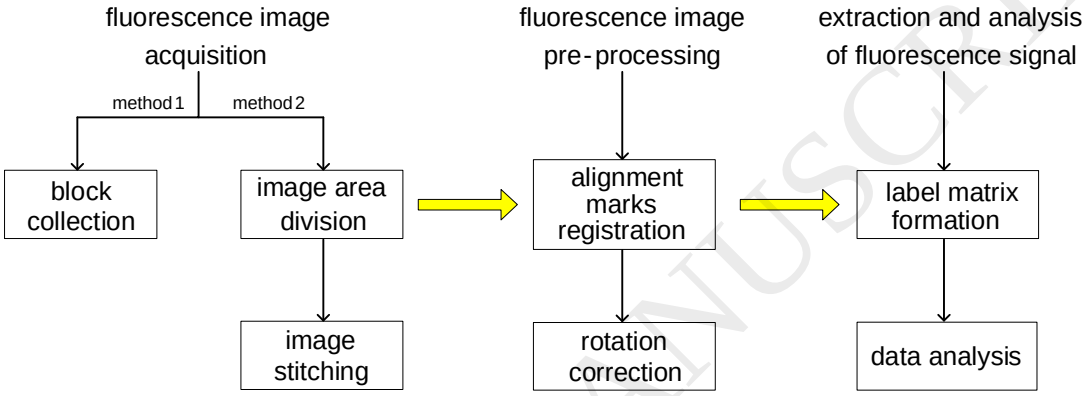

Figure 2 dPCR chip fluorescence signal detection and analysis method flow chart.

The chip layout was divided into six blocks and we then captured two sets of images using a microscope objective lens with a magnification of 2.5×. The first set had six images captured using the fluorescence mode and the second set had six images captured using the BF imaging method, which was used to locate the chip on the microscope stage using the alignment marks. The images were pre-processed, and the fluorescence signal was extracted for each reaction well.

Method 2: Stitching

Partial images captured in fluorescence mode were indexed and the entire image of the dPCR chip was obtained by stitching together the partial images using a microscope objective lens with a magnification of 5×. The microscope stage location was controlled by a human–computer interaction system. Partial images were acquired automatically in a progressive scanning manner with at least one row/column of reaction wells having overlapping margins S_2. These overlapping margins were used to identify the position of each image and the position of the stitched partial images. Then, we set the block with a width of 10 pixels for comparison of those two overlapping images starting at the position S_3:

$$S_3 = n - S_2 - r/2,\ S_3 > S_2, \quad (1)$$

where n is the column size of each chip image captured by a camera attached to a microscope and r is the extended distance from the overlapping edges. We then compared the overlapping parts of the two images to get the correlation matrix and extracted the most relevant matching before performing the image stitching. The image stitching of two images from a chip with a well diameter of 20 μm is shown in Figure 3.

We generally used the block method to determine the number of PCR wells containing amplified DNA from all chips. Image processing from the dPCR chip with 5 μm wells hit the method limit as there were only ≈ 33.2

pixels per well. The stitching method would have to be used for layouts with higher densities as it is more general, however, this requires longer processing times. In our work, we mostly focused on the block method.

2.5. Fluorescence image pre-processing

After obtaining the entire image of the dPCR chip, we registered the six alignment marks using the image recognition database created by the image acquisition tool in MATLAB. Then, we looked for the edges of the alignment marks using the Canny operator with a threshold of [0.01 0.3] and a default sigma value and detected the edge lines using the Hough transform. Finally, the intersecting points of four edge lines were calculated based on the analytic geometric algorithm. The coordinates of the center of each alignment mark were automatically calculated $P_i(x_i, y_i)$, $i = 1 \ldots 6$) and, subsequently, the image rotation was determined:

$$\alpha_i = tan\frac{|y_{2i}-y_{2i-1}|}{|x_{2i}-x_{2i-1}|}, \; i = 1, 2, 3, \tag{2}$$

$$\alpha_{j+3} = tan\frac{|x_j-x_{j+2}|}{|y_j-y_{j+2}|}, \; j = 1, 2, 3, 4, \tag{3}$$

$$\alpha_{k+7} = tan\frac{|x_k-x_{k+4}|}{|y_k-y_{k+4}|}, \; k = 1, 2, \tag{4}$$

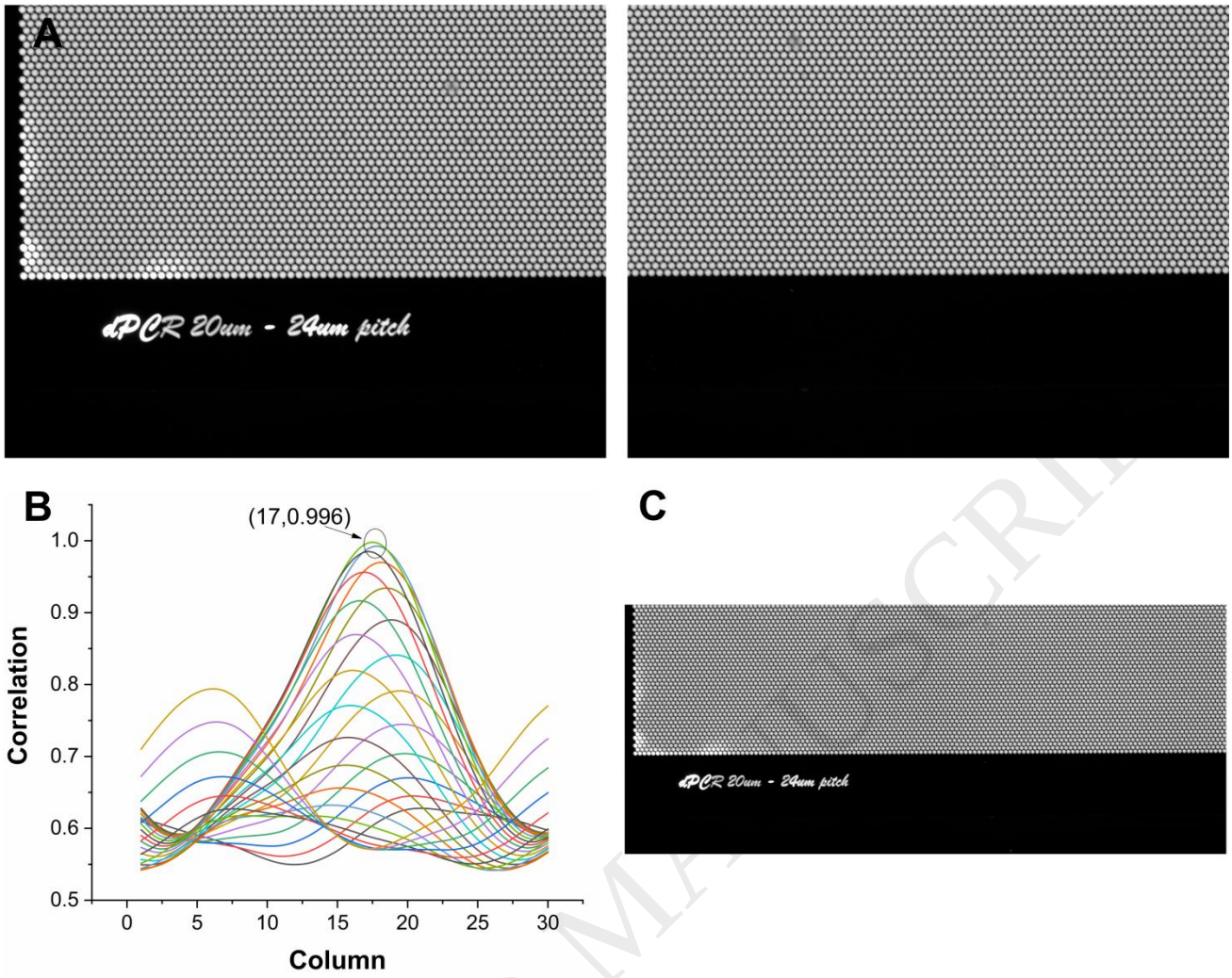

Figure 3 Example of stitching two images. (A) Two images used as input. (B) We determined the most correlated column and row from two adjacent overlapped images with values of 17 and 12, respectively, via the maximum correlation value and saved them in the matrix in MATLAB. The maximum correlation value was ≈0.996. (C) Then, we formed the merged image.

where $\sum_{l=1}^{3}\alpha_l$ is the corresponding sum of angles between P_1 and P_2, P_3 and P_4, and P_5 and P_6 in the horizontal direction and $\sum_{l=4}^{9}\alpha_l$ is the corresponding sum of angles between P_1 and P_3, P_3 and P_5, P_2 and P_4, P_4 and P_6, P_1 and P_5, and P_2 and P_6 in the vertical direction.

After calculating the average values of $\overline{\alpha_x}=\frac{\sum_{l=1}^{3}\alpha_l}{3}$ in the horizontal and $\overline{\alpha_y}=\frac{\sum_{l=4}^{9}\alpha_l}{6}$ in the vertical directions, we obtained the average rotation angle $\alpha=\frac{\overline{\alpha_x}+\overline{\alpha_y}}{2}$ of the complete image, thereby reducing the error of the rotation angle. Removal of α from the image placed it into its correct orientation.

2.6. Extraction and analysis of fluorescence signal

We created an array of reaction wells in the MATLAB environment according to the layout of the respective dPCR chip and transform it into a matrix with reaction wells matched the location of the wells on the actual chip. The matrix was defined with two levels of gray and all pixels within the well had the same amplitude of gray. All the gray levels of the pixels in areas outside of the wells were set to zero. Then, we numbered all the reaction wells in sequence and compared the corresponding wells from the matrix with the wells from an actual

fluorescence image of the dPCR chip to obtain the fluorescence intensity in each reaction well. This method of determination of reaction well location suppressed the potential interference induced by fluorescence noise outside of the reaction wells.

We processed the fluorescence image of the dPCR chip by using a histogram to determine the frequency of occurrence as a function of normalized fluorescence intensity to present the amplification result of the dPCR. The histogram of the gray levels in the fluorescence image consisted of two peaks. The peak with the lower value of mean fluorescence amplitude represented the number of reaction wells with no PCR amplification (NW), while the second peak with the higher mean value of fluorescence amplitude represented the number of reaction wells with amplified DNA (PW).

2.7. Speed of the digital image processing algorithms

An essential advantage of our implemented image processing is the speed of the evaluation based on the algorithms mentioned above due to the code optimization. Most of the calculations were optimized for matrix manipulations, a known strong feature in the MATLAB software. We needed time < 1.2 min to capture all six fluorescence images using camera resolution of 5472 × 3648 pixels and processing them creating final image with the size of 9388 × 8747 pixels (*Method 1*). That corresponds to shortening image processing more than three times [43]. The most time-consuming code portions obtained by the profiling of the m-scripts were optimized in the form of *.mex files (MATLAB executable file). This resulted in speed improvements of approximately two orders of magnitude in terms of the computing time. As an example, the speed of the evaluation on a notebook with four core i7-4700mq 2.40 GHz CPU and 16 GB RAM was < 3 s using MATLAB R2018a under a 64-bit Windows 7 operating system. Further speed improvement could be achieved by using a greater number of cores, a graphics card, or field programmable gate arrays.

3. Results and Discussion

3.1. PCR chips

The physical sizes of the family of designed silicon chips with different resolutions are shown in Table 1. These dPCR chips will greatly enhance the dPCR implementation process because users can adjust the resolution according to the specific application, such as circulating tumor DNA detection or prenatal diagnostics, without changing the dPCR platform.

Table 1 Physical sizes of four different dPCR chips.

Well diameter (μm)	Total number of wells	Number of wells in one segment	Total volume (μL)	Volume of a single well (pL)
50	26,448	4,408	1.560432	59
20	139,896	23,316	0.839376	6
10	475,272	79,212	0.370712	0.78
5	1,656,000	276,000	0.165600	0.1

The key challenges of the cdPCR system are the sample distribution evenness, sample cross-contamination, and sample evaporation during thermal cycling. We developed a chip surface treatment recipe, a sample loading method, and a chip packaging technique to suppress but not eliminate these problems.

3.2. DNA template

As a DNA template, we selected a fragment with 207 base pairs (bp) of cyclin-dependent kinase inhibitor 2A (CDKN2A). This fragment is associated with pancreatic cancer and can be used to perform the detection of circulating tumor DNA. The total length of the amplicon was 120 bp. The sequences of the gene, the forward and reverse primers, and the FAM probe are listed below.

DNA template

AGCGGGAGCAGGGGATGGCGGGCGACTCTGGAGGACGAAGTTTGCAGGGGAATTGGAATCAGG
TAGCGCTTCGATTCTCCGGAAAAAGGGGAGGCTTCCTGGGGAGTTTTCAGAAGGGGTTTGTAATC
ACAGACCTCCTCCTGGCGACGCCCTGGGGGCTTGGGAAGCCAAGGAAGAGGAATGAGGAGCCA
CGCGCGTACAGATCTC

Primers

Forward primer: 5'-CGACTCTGGAGGACGAAGT-3'

Reverse primer: 5'-AGGAGGAGGTCTGTGATTACAA-3'

FAM probe: 5'-AATCAGGTAGCGCTTCGATTCTCCG-3' (BHQ1)

The DNA PCR master mix was prepared by mixing ≈ 0.5 µL Taq polymerase with ≈ 2 µL buffer and adding ≈ 0.8 µL dNTP and ≈ 0.4 µL of forward and reverse primers, respectively; ≈ 0.4 µL of FAM probe; and ≈ 1 µL of the DNA template. Finally, the solution volume was adjusted to ≈ 10 µL by adding ≈ 4.5 µL of deionized H_2O. Due to an unfavorable surface-to-volume ratio of the well, we increased the concentration of the polymerase to five times the previously suggested amount [44].

3.3. PCR protocol

We performed a two-step PCR protocol based on "Taqman chemistry" [45] using a 6-carboxyfluorescein (FAM) probe. We used a script in the LabView environment for temperature control that consisted of two parts: (1) activating the polymerase at a set temperature of ≈ 95°C with a duration of ≈ 120 s; and (2) continuing with 45 cycles of PCR amplification consisting of two temperature steps, denaturation at ≈ 95°C for ≈ 8 s, and annealing at ≈ 52°C for ≈ 30 s.

3.4. Results of fluorescence image processing

After completing the PCR, we captured the chip image by using both the bright field (BF) and fluorescence modes of a CMOS camera.

Method 1: First, we captured six images (one per block) and stitched them together. Then, we found and registered six alignment marks, rotated the image, and extracted fluorescence mean values for all wells.

Method 2: First, we acquired 63 partial images and then stitched all of them into a single image of the entire dPCR chip (Figure 4A). Next, we determined the coordinates of the six alignment marks' centers using the Canny operator and Hough transform (Figure 4B) and then rotated the image by α calculated in Section 3.3.2 (Figure 4C). Then, the image was compared with "matrix," as shown in Figure 4D. Here, we can see that the wells in the matrix are located within the wells from the actual image with a high level of matching. Thus, the fluorescence intensity of each reaction well can be extracted, and reaction wells can be segmented to locate their position and boundaries and to determine their mean values of fluorescence intensity.

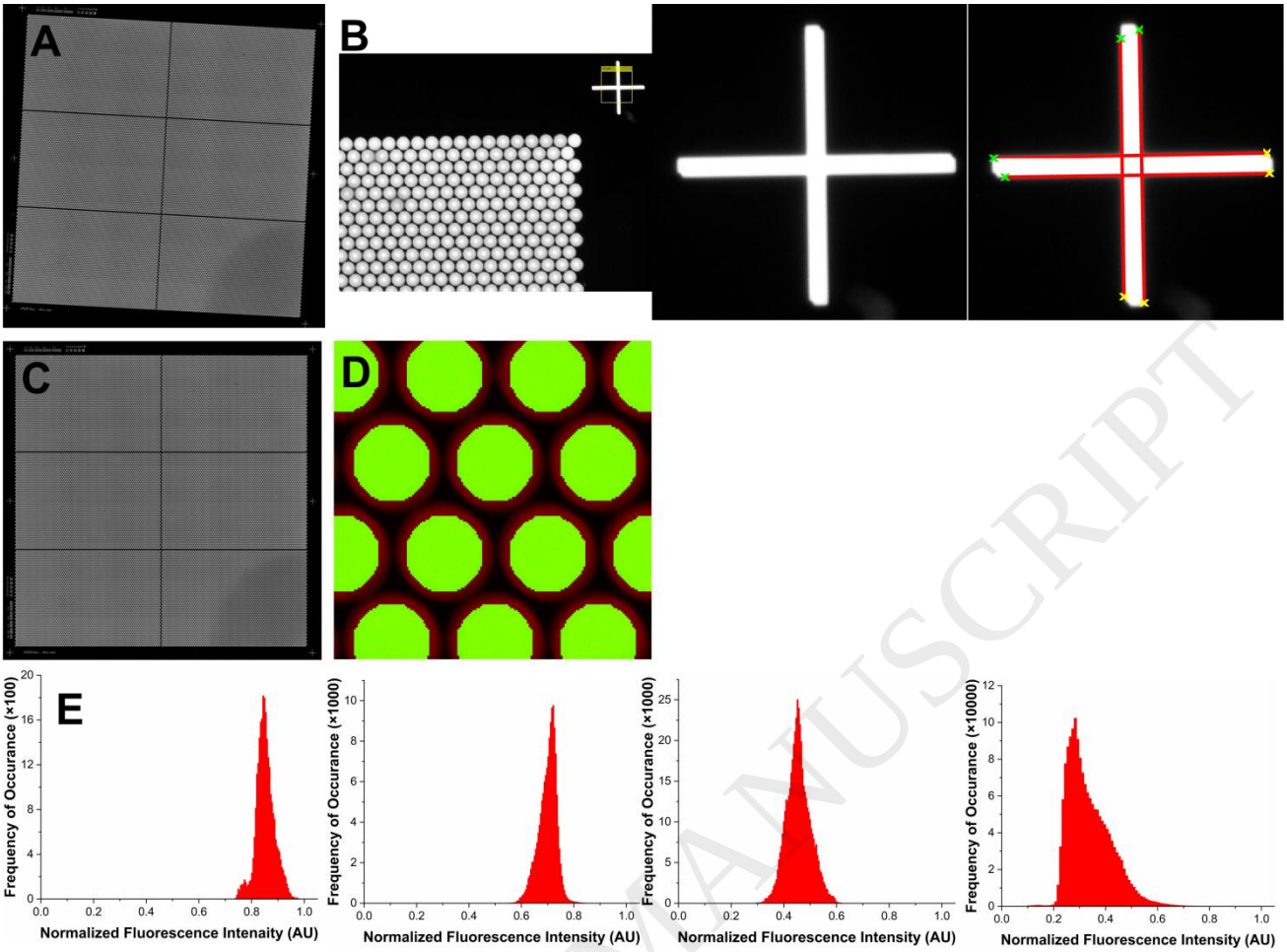

Figure 4 (A) Complete image of the dPCR chip filled with fluorescein and consisting of 63 individual images. (B) Cross marks' center registration. (C) Image after the rotation correction. (D) "Matrix" (green) and the obtained fluorescence image (red). (E) Histograms of normalized fluorescence intensities of chips with well diameters of (from left to right) 50 µm, 20 µm, 10 µm, and 5 µm.

According to the method presented in this paper, we verified these results by using chips with various well diameters filled with fluorescein and obtained a histogram of the frequency of occurrence with normalized fluorescence intensities (Figure 4E). We also used a chip with a well diameter of 50 µm using a fragment of DNA of cyclin-dependent kinase inhibitor 2A (CDKN2A), which is associated with pancreatic cancer, with its initial content (C) of 67 ng·µL^{-1}. We prepared three different solutions, each with a volume of ≈ 10 µL, which were even mixtures of the PCR master mix and different DNA numbers of copies (λ) (1,030,000, 103,000, and 1,030). Values of λ were calculated according to the formula [46]:

$$\lambda = \frac{C \cdot A}{DNA\ Length \cdot 10^9 \cdot 650}\ , \tag{5}$$

where A is an Avogadro's number and 650 is the average molecular weight of a DNA base pair. The chip has a calculated volume of ≈ 1.56 µL, therefore, after filling wells with the master mix solution containing the DNA template, the resulting DNA copy numbers on the chip are ≈ 160,680, ≈ 16,068, and ≈ 161. Conveniently, the formula has also been available as an online calculator since 2004 [47]. Per Poisson distribution, the most probable number of wells containing DNA (k) was calculated as [36]:

$$k = \left(1 - e^{-\lambda}\right) \cdot n, \tag{6}$$

where n is the number of reaction wells. We obtained values of PWs in one block of ≈ 4,397, ≈ 1,989, and ≈ 26.

Table 2 DNA copy numbers in the chip and the calculated probability of occurrence of PWs and NWs per Poisson distribution in one block.

Number of DNA copies in the chip	Average copy number of DNA per well	Calculated/measured PWs per block	Calculated/measured NWs per block	Calculated PWs/NWs ratio	Measured PWs/NWs ratio
160,680	6	4,397/4,343	11/65	400	66.82
16,068	0.6	1,989/1,926	2,419/2,482	0.82	0.78
161	0.006	26/23	4,382/4,385	0.006	0.005

We captured the image of one block of dPCR chips loaded with different copy numbers of the DNA template (≈ 160,680, ≈ 16,068, and ≈ 161) corresponding to the average DNA copy numbers in one well of ≈ 6, ≈ 0.6, and ≈ 0.006. Subsequently, we extracted the fluorescence amplitudes from each well (Figure 5). The wells with higher fluorescence amplitudes were PWs and the wells with lower fluorescence amplitude were NWs. Then, we built the histogram to show the frequency of fluorescence amplitude occurrence per reaction well and

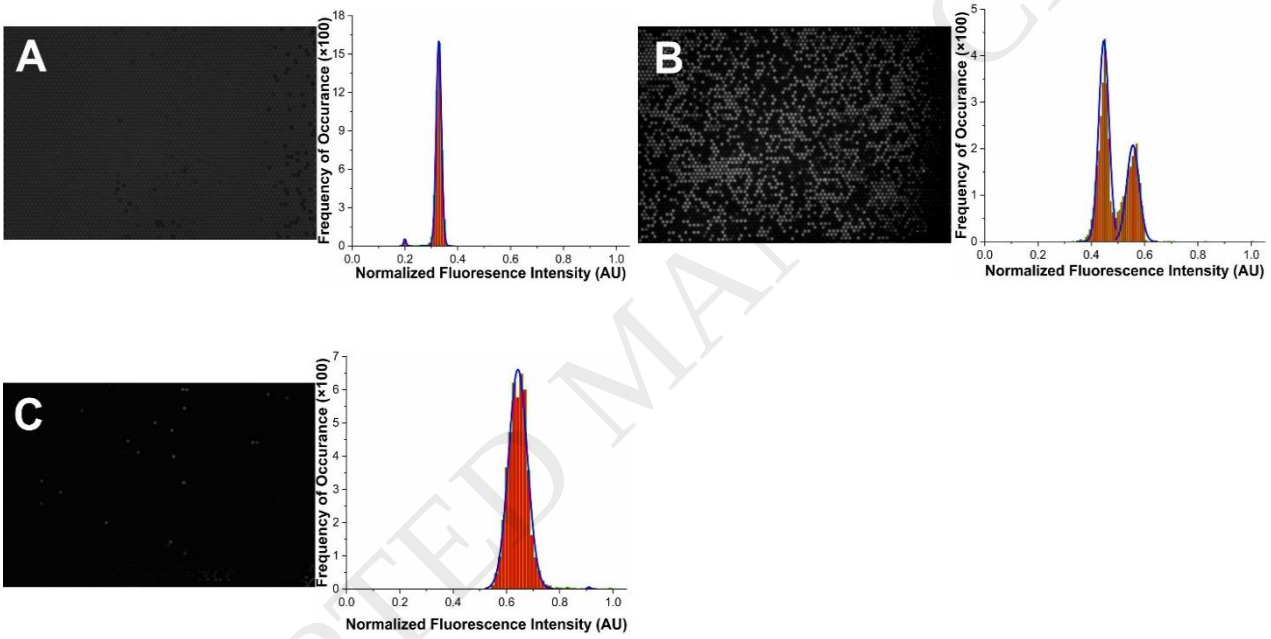

Figure 5 Fluorescence signal analysis result after PCR in a chip block with a well diameter of 50 μm. (A) Image of a single block with a template copy number of ≈ 160,680, resulting in ≈ 6 copies per well per Poisson distribution. The histogram shows two peaks with normalized mean values of fluorescence of ≈ 0.21 and ≈ 0.35. (B) Image of a single block of the dPCR chip with a copy number of ≈ 16,068, resulting in ≈ 0.6 copies per well. The histogram shows two peaks with normalized mean values of fluorescence of ≈ 0.45 and ≈ 0.56. (C) Image of a single block of the dPCR chip with a copy number of ≈ 161, resulting in ≈ 0.006 copies per well. The histogram shows two peaks with normalized mean values of fluorescence of ≈ 0.64 and ≈ 0.91.

extracted the ratio between number of PWs and NWs and obtained 66.82, 0.78, and 0.005 for the DNA average copy numbers of ≈ 6, ≈ 0.6, and ≈ 0.006, respectively.

The ratios of 400, 0.82, and 0.006 based on the Poisson distribution (Table 2) match the ratios extracted from the histograms. The minor differences might have been caused by water evaporation during thermal cycling along the chip edge.

4. Conclusions

We proposed a design of a digital PCR chip and a method to process and analyze the results from its fluorescence image using a MATLAB script and experimentally verified both. The chip layout was divided into six blocks and we acquired corresponding fluorescence images from each block while registering alignment marks and correcting their rotations. Then, we located all reaction wells, calculated their average amplitudes of fluorescence, built a histogram, and determined the number of PWs and NWs. This method can quantitatively obtain the dPCR results based on a user-friendly interface. Our method of fluorescence image processing can also be applied for array-based microfluidics used in instruments utilizing digital microfluidics for rapid biomedical diagnoses [48], including portable platforms[49].

The system can also be improved by eliminating "non-performing wells" detected during chip fabrication. The chip can be filled with the fluorescein solution and its fluorescence image can be captured and processed. We could also extract the fluorescence intensity as a function of location and then perform the image normalization. Subsequently, the wells with fluorescence amplitudes that deviated from the mean value by more than a predefined tolerance would be registered and later ignored.

Acknowledgments

This work was supported by the "Foreign Experts Program" of P.R. China (W099109). The authors are grateful to Mr. Chaofei Yang from the School of Life Science of Northwestern Polytechnical University, Xian, P.R. China and to Dr. Giuseppina Simone from the School of Mechanical Engineering for sequence testing and the fruitful discussions regarding the experiment. This work was also partially supported by the Grant Agency of the Czech Republic under the contract GA16-11140S. We also thank Dr. Bojan Ilic from the National Institute of Standards and Technology, Gaithersburg, USA for his help with the original chip's layout design and fabrication.

Supplementary material

A script defining the chip layout.

References

[1] R. Saiki, S. Scharf, F. Faloona, K. Mullis, G. Horn, H. Erlich, et al., Enzymatic amplification of beta-globin genomic sequences and restriction site analysis for diagnosis of sickle cell anemia, Science, 230(1985) 1350-4.

[2] M.A. Valasek, J.J. Repa, The power of real-time PCR, Adv Physiol Educ, 29(2005) 151-9.

[3] R. Higuchi, C. Fockler, G. Dollinger, R. Watson, Kinetic PCR Analysis: Real-time Monitoring of DNA Amplification Reactions, Bio/Technology, 11(1993) 1026–30.

[4] B. Vogelstein, K.W. Kinzler, Digital PCR, Proc Natl Acad Sci U S A, 96(1999) 9236-41.

[5] S. Ono, S. Lam, M. Nagahara, D. Hoon, Circulating microRNA Biomarkers as Liquid Biopsy for Cancer Patients: Pros and Cons of Current Assays, Journal of Clinical Medicine, 4(2015) 1890-907.

[6] A. Pender, I. Garcia-Murillas, S. Rana, R.J. Cutts, G. Kelly, K. Fenwick, et al., Efficient Genotyping of KRAS Mutant Non-Small Cell Lung Cancer Using a Multiplexed Droplet Digital PCR Approach, PLOS ONE, 10(2015) e0139074.

[7] T. Demeke, T. Graefenhan, M. Holigroski, U. Fernando, J. Bamforth, S.-J. Lee, Assessment of droplet digital PCR for absolute quantification of genetically engineered OXY235 canola and DP305423 soybean samples, Food Control, 46(2014) 470-4.

[8] M. Hussain, R. Fantuzzo, S. Mercorelli, C. Cullen, A direct droplet digital PCR method for quantification of residual DNA in protein drugs produced in yeast cells, Journal of Pharmaceutical and Biomedical Analysis, 123(2016) 128-31.

[9] T. Demeke, M. Holigroski, M. Eng, J. Xing, Absolute quantification of genetically engineered traits with droplet digital PCR: Effect of DNA treatments and spiking with non-target DNA, Food Control, 68(2016) 105-11.
[10] H.C. Fan, Y.J. Blumenfeld, Y.Y. El-Sayed, J. Chueh, S.R. Quake, Microfluidic digital PCR enables rapid prenatal diagnosis of fetal aneuploidy, American Journal of Obstetrics and Gynecology, 200(2009).
[11] R. Sanders, J.F. Huggett, C.A. Bushell, S. Cowen, D.J. Scott, C.A. Foy, Evaluation of Digital PCR for Absolute DNA Quantification, Anal Chem, 83(2011) 6474-84.
[12] C.M. Hindson, J.R. Chevillet, H.A. Briggs, E.N. Gallichotte, I.K. Ruf, B.J. Hindson, et al., Absolute quantification by droplet digital PCR versus analog real-time PCR, Nature Methods, 10(2013) 1003-5.
[13] J. Camunas-Soler, H. Lee, L. Hudgins, S.R. Hintz, Y.J. Blumenfeld, Y.Y. El-Sayed, et al., Noninvasive Prenatal Diagnosis of Single-Gene Disorders by Use of Droplet Digital PCR, Clinical Chemistry, 64(2018) 336-45.
[14] Y. Uchiyama, M. Nakashima, S. Watanabe, M. Miyajima, M. Taguri, S. Miyatake, et al., Ultra–sensitive droplet digital PCR for detecting a low–prevalence somatic GNAQ mutation in Sturge–Weber syndrome, Scientific Reports, 6(2016) 22985.
[15] J.A. Denis, A. Patroni, E. Guillerm, D. Pepin, N. Benali-Furet, J. Wechsler, et al., Droplet digital PCR of circulating tumor cells from colorectal cancer patients can predict KRAS mutations before surgery, Molecular Oncology, 10(2016) 1221-31.
[16] N.J. Heredia, P. Belgrader, S. Wang, R. Koehler, J. Regan, A.M. Cosman, et al., Droplet Digital (TM) PCR quantitation of HER2 expression in FFPE breast cancer samples, Methods, 59(2013) S20-S3.
[17] A.L. Reid, J.B. Freeman, M. Millward, M. Ziman, E.S. Gray, Detection of BRAF-V600E and V600K in melanoma circulating tumour cells by droplet digital PCR, Clinical Biochemistry, 48(2015) 999-1002.
[18] D. Sefrioui, N. Sarafan-Vasseur, L. Beaussire, M. Baretti, A. Gangloff, F. Blanchard, et al., Clinical value of chip-based digital-PCR platform for the detection of circulating DNA in metastatic colorectal cancer, Digestive and Liver Disease, 47(2015) 884-90.
[19] M.M. Ahmad, A.B. Jambek, M.Y. bin Mashor, Ieee, Image Gridding Algorithm for DNA Microarray Analyser, 2016 3rd International Conference on Electronic Design2016, pp. 452-7.
[20] B. Belean, R. Terebes, A. Bot, Low-complexity PDE-based approach for automatic microarray image processing, Medical & Biological Engineering & Computing, 53(2015) 99-110.
[21] Y. Li, A. Paun, M. Paun, Improvements on contours based segmentation for DNA microarray image processing, Theoretical Computer Science, 701(2017) 174-89.
[22] E. Ensink, J. Sinha, A. Sinha, H. Tang, H.M. Calderone, G. Hostetter, et al., Segment and Fit Thresholding: A New Method for Image Analysis Applied to Microarray and Immunofluorescence Data, Anal Chem, 87(2015) 9715-21.
[23] D. Chakraborty, G. Sen, S. Hazra, Image Segmentation Techniques: LAP LAMBERT Academic Publishing; 2013.
[24] A.E. El-Baz, Jiang, X. (Ed.), Suri, J. (Ed.). , Biomedical Image Segmentation, Boca Raton: CRC Press; 2017.
[25] G. Weng, cDNA Microarray Image Processing Using Mathematical Morphological Segmentation, in: J. Chen (Ed.) Proceedings of the 29th Chinese Control Conference2010, pp. 2660-4.
[26] V. Uslan, I.O. Bucak, Ieee, Clustering-based Spot Segmentation of cDNA Microarray Images, 2010 Annual International Conference of the Ieee Engineering in Medicine and Biology Society2010, pp. 1828-31.
[27] Z. Wang, B. Zineddin, J. Liang, N. Zeng, Y. Li, M. Du, et al., cDNA microarray adaptive segmentation, Neurocomputing, 142(2014) 408-18.
[28] T.N. Wang, T.J. Li, G.F. Shao, S.X. Wu, An improved K-means clustering method for cDNA microarray image segmentation, Genetics and Molecular Research, 14(2015) 7771-81.
[29] P. Buenestado, L. Acho, Image Segmentation Based on Statistical Confidence Intervals, Entropy, 20(2018) 46.
[30] H. Ajmal, S. Rehman, U. Farooq, Q.U. Ain, F. Riaz, A. Hassan, Convolutional neural network based image segmentation: a review, SPIE Defense & Security, SPIE2018, p. 13.

[31] Y. Guo, Y. Liu, T. Georgiou, M.S. Lew, A review of semantic segmentation using deep neural networks, International Journal of Multimedia Information Retrieval, 7(2018) 87-93.
[32] S. Katsigiannis, E. Zacharia, D. Maroulis, Grow-Cut Based Automatic cDNA Microarray Image Segmentation, IEEE Transactions on Nanobioscience, 14(2015) 138-45.
[33] A.K. Helmy, G.S. El-taweel, Regular gridding and segmentation for microarray images, Computers & Electrical Engineering, 39(2013) 2173-82.
[34] E. Zacharia, D. Maroulis, An original genetic approach to the fully automatic gridding of microarray images, IEEE Transactions on Medical Imaging, 27(2008) 805-13.
[35] K.A. Mendhurwar, R. Kakumani, V. Devabhaktuni, Ieee, Microarray Image Segmentation Using Chan-Vese Active Contour Model and Level Set Method, 2009 Annual International Conference of the Ieee Engineering in Medicine and Biology Society, Vols 1-202009, pp. 3629-32.
[36] K.A. Heyries, C. Tropini, M. VanInsberghe, C. Doolin, O.I. Petriv, A. Singhal, et al., Megapixel digital PCR, Nature Methods, 8(2011) 649-U64.
[37] P. Neuzil, C.D.M. Campos, C.C. Wong, J.B.W. Soon, J. Reboud, A. Manz, From chip-in-a-lab to lab-on-a-chip: towards a single handheld electronic system for multiple application-specific lab-on-a-chip (ASLOC), Lab on a Chip, 14(2014) 2168-76.
[38] P. Neuzil, L. Novak, J. Pipper, S. Lee, L.F.P. Ng, C. Zhang, Rapid detection of viral RNA by a pocket-size real-time PCR system, Lab on a Chip, 10(2010) 2632-4.
[39] C.D. Ahrberg, B.R. Ilic, A. Manz, P. Neuzil, Handheld real-time PCR device, Lab on a Chip, 16(2016) 586-92.
[40] C.D. Ahrberg, A. Manz, P. Neuzil, Palm-Sized Device for Point-of-Care Ebola Detection, Analytical Chemistry, 88(2016) 4803-7.
[41] K.C. Balram, D.A. Westly, M. Davanco, K. Grutter, Q. Li, T. Michels, et al., The Nanolithography Toolbox, J Res Natl Inst Stand, 121(2016) 464-75.
[42] F. Laerme, A. Schilp, K. Funk, M. Offenberg, Bosch deep silicon etching: improving uniformity and etch rate for advanced MEMS applications, (1999) 211-6.
[43] Y. Men, Y. Fu, Z. Chen, P.A. Sims, W.J. Greenleaf, Y. Huang, Digital Polymerase Chain Reaction in an Array of Femtoliter Polydimethylsiloxane Microreactors, Analytical Chemistry, 84(2012) 4262-6.
[44] J. Hoffmann, M. Trotter, F. von Stetten, R. Zengerle, G. Roth, Solid-phase PCR in a picowell array for immobilizing and arraying 100 000 PCR products to a microscope slide, Lab on a Chip, 12(2012) 3049-54.
[45] P.M. Holland, R.D. Abramson, R. Watson, D.H. Gelfand, Detection of specific polymerase chain reaction product by utilizing the 5'----3' exonuclease activity of Thermus aquaticus DNA polymerase, Proc Natl Acad Sci U S A, 88(1991) 7276-80.
[46] V.A. Morozov, A.V. Morozov, A. Rotem, U. Barkai, S. Bornstein, J. Denner, Extended Microbiological Characterization of Göttingen Minipigs in the Context of Xenotransplantation: Detection and Vertical Transmission of Hepatitis E Virus, PLOS ONE, 10(2015) e0139893.
[47] A. Staroscik, Calculator for determining the number of copies of a template, 2004.
[48] K. Choi, A.H.C. Ng, R. Fobel, A.R. Wheeler, Digital Microfluidics, Annual Review of Analytical Chemistry, 5(2012) 413-40.
[49] E. Samiei, M. Tabrizian, M. Hoorfar, A review of digital microfluidics as portable platforms for lab-on a-chip applications, Lab on a Chip, 16(2016) 2376-96.